

Magnetic Skyrmions in FePt Square-Based Nanoparticles Around Room-Temperature

Christos Tyrpenou¹, Vasileios D. Stavrou¹, and Leonidas N. Gergidis^{*1}

¹Department of Materials Science and Engineering, University of Ioannina, 45110 Ioannina, Greece

September 13, 2022

Abstract

Magnetic skyrmions formed at temperatures around room temperature in square-based parallelepiped magnetic FePt nanoparticles with perpendicular magnetocrystalline anisotropy (MCA) were studied during the magnetization reversal using micromagnetic simulations. Finite Differences (FD) method were used for the solution of the Landau-Lifshitz-Gilbert equation. Magnetic configurations exhibiting Néel skyrmionic formations were detected. The magnetic skyrmions can be created in different systems generated by the variation of external field, side length and width of the squared-based parallelepiped magnetic nanoparticles. Micromagnetic configurations revealed a variety of states which include skyrmionic textures with one distinct skyrmion formed and being stable for a range of external fields around room-temperature. The size of the formed Néel skyrmion is calculated as a function of the external field, temperature, MCA and nanoparticle's geometrical characteristic lengths which can be adjusted to produce Néel type skyrmions on demand having diameters down to 12 nm. The micromagnetic simulations revealed that stable skyrmions at the temperature range 270 - 330 K can be created for FePt magnetic nanoparticle systems lacking of chiral interactions such as Dzyaloshinskii-Moriya.

1 Introduction

Magnetic skyrmions are considered by many researchers as dynamic candidates for next generation high density efficient information encoding providing enhanced capabilities in magnetic writing and storage [1, 2, 3, 4, 5]. Their small size and the low current density needed for their manipulation and control [6] pave the way for potential engineering applications. Over the last decade magnetic skyrmions have been under intense theoretical, computational and experimental investigation [7, 8, 9, 10, 11, 12, 13, 14, 15]. It is of significant importance to understand how the confined nature of geometry can affect skyrmion creation-stabilization [16, 17, 18] and consequently the size and energetics of the skyrmionic states.

Recently, Fert and his collaborators [19] combined concomitant magnetic force microscopy and Hall resistivity measurements to demonstrate the electrical detection of sub-100 nm skyrmions in a multilayered thin film at room-temperature. Additionally, Legrand et al. [20] showed that room temperature antiferromagnetic skyrmions can be stabilized in synthetic antiferromagnets (SAFs), in which perpendicular magnetic anisotropy, antiferromagnetic coupling and chiral order can be adjusted concurrently. In up to date reports room-temperature magnetic skyrmions in ultrathin magnetic multilayer structures of Co/Pd [21], Pt/Co/MgO [22] and Co/Ni [23] were reported. Brändao et al. [24] reported on the evidence of skyrmions in unpatterned symmetric Pd/Co/Pd multilayers at room temperature without prior application of neither electric current nor magnetic field. Husain et al. [25] observed stable skyrmions in unpatterned Ta/Co₂FeAl(CFA)/MgO thin film heterostructures at room temperature in remnant state employing magnetic force microscopy showing that these skyrmions consisting of ultrathin ferromagnetic CFA Heusler alloy result from strong interfacial Dzyaloshinskii-Moriya interaction (i-DMI). Ma et al. [26] employed atomistic stochastic Landau-Lifshitz-Gilbert simulations to investigate skyrmions in amorphous ferrimagnetic GdCo revealing that a significant reduction in DMI below that of Pt is sufficient to stabilize ultrasmall skyrmions even in films as thick as 15 nm.

In the present simulation work, the formation of magnetic skyrmions around room-temperature in the external field range used for the magnetization reversal in a single FePt nanoparticle having parallelepiped geometry of square base is studied. The current research effort was inspired-initiated by the variety of skyrmionic magnetic textures detected in FePt triangular and reuleaux prismatic nanoparticles encapsulating multiple skyrmions at

*lgergidi@uoi.gr; lgergidis@gmail.com

0 K using Finite Elements micromagnetics simulations [27, 28, 29]. It was shown that for magnetocrystalline anisotropy (MCA) values between $Ku = 200 - 500$ kJ/m³ three distinct skyrmions are formed and persist for a range of external fields along with rich magnetic structures in the bulk of the FePt nanoparticle similar to those observed in DMI stabilized systems [30]. Néel type skyrmionic textures were detected on the Reuleaux geometry's bases coexisting with Bloch-type textures in the bulk of the FePt nanoelement. It was also shown that the size of skyrmions depends linearly on the field value B_{ext} and that the slope of the linear curve can be controlled by MCA value [29]. Single layered square-based FePt nanoparticles in the absence of chiral interactions like Dzyaloshinskii-Moriya (DM) or its interfacial analogue (iDM) (present in multi-layered hetero-structures with spin-orbit coupling) are investigated. Skyrmionic textures and formations are explored along with the underlying physical mechanisms for temperatures around 300 K and for different geometrical characteristics of the nanoparticle.

2 Micromagnetic modeling

The Landau-Lifshitz-Gilbert (LLG) equation governs the rate of change of the dynamical magnetization field \mathbf{M} and is given by the relation

$$\frac{d\mathbf{M}}{dt} = \frac{\gamma}{1 + \alpha^2}(\mathbf{M} \times \mathbf{B}_{eff}) - \frac{\alpha\gamma}{(1 + \alpha^2)|\mathbf{M}|}\mathbf{M} \times (\mathbf{M} \times \mathbf{B}_{eff}). \quad (1)$$

The quantity $\alpha > 0$ is a phenomenological dimensionless damping constant that depends on the material and γ is the electron gyromagnetic ratio. The effective field that governs the dynamical behavior of the system has contributions from various effects that are of very different nature and can be expressed as $\mathbf{B}_{eff} = \mathbf{B}_{ext} + \mathbf{B}_{exch} + \mathbf{B}_{anis} + \mathbf{B}_{demag} + \mathbf{B}_{thermal}$. Respectively, these field contributions are the external field \mathbf{B}_{ext} , the exchange field \mathbf{B}_{exch} , the anisotropy field \mathbf{B}_{anis} , the demagnetizing field \mathbf{B}_{demag} and the thermal field $\mathbf{B}_{thermal}$.

In particular, the thermal field $\mathbf{B}_{thermal}$ which incorporates implicitly the temperature can be expressed by $\mathbf{B}_{thermal}(t) = \mathbf{n}(t)\sqrt{\frac{2\mu_0\alpha k_B T}{B_{sat}\gamma\Delta V\Delta t}}$ according to Brown [31]. In thermal field expression α is the aforementioned damping constant, μ_0 is the vacuum permeability constant, k_B is the Boltzmann constant, T is the temperature (throughout manuscript slightly slanted T is used for temperature), B_{sat} the saturation magnetization expressed in Tesla (T), ΔV the cell volume, Δt the time step and \mathbf{n} a random vector generated from a standard normal distribution whose value is changed every time step. For the solution of the LLG equation micromagnetic Finite Differences (FD) calculations have been conducted using Mumax3 Finite Differences software [32, 33]. The dimensionless damping constant α was set to 1 in order to achieve fast damping and reach convergence quickly as we are interested in static magnetization configurations. The time step used for the integration of the LLG equation was equal to $\Delta t = 1$ fs.

The square-based nanoparticle having side length $a = 150$ nm and width $w = 36$ nm will be considered as the reference nanoparticle and will be used for the multi-parametric investigation conducted in the present work. It is chosen since it encapsulates the most stable skyrmion with respect to the magnetic field range and skyrmion type as it will be made clear in the sequel. The particular width value $w = 36$ nm is selected following previous studies [27, 28, 29] which focus on FePt triangular and reuleaux prismatic nanoelements. In addition, the 36 nm thickness of nanoparticle matches that reported in [34]. For the objectives of the multi-parametric study additional magnetic samples-nanoparticles with parallelepiped geometry of square base with varying side length a from 40 to 180 nm and w ranging from 6 to 36 nm were also used. The following frame of reference axes assignment convention was used: x, y along the square's edges, and z perpendicular to the nanoparticle's square base. The mesh used for the discrete representation of the rectangular parallelepiped nanoparticle under study was a regular 3D mesh with characteristic discretization lengths $\Delta x = \Delta y = 2$ nm, $\Delta z = 1$ nm in x, y, z -directions respectively. The lengths $\Delta x, \Delta y, \Delta z$ used for the discretization of the rectangular domain under investigation were lower than the exchange length $l_{ex} = \sqrt{\frac{2A}{\mu_0 M_s^2}} \approx 3.5$ nm for the FePt magnetic material.

The material parameters used in this study have been reduced accordingly in order to follow their temperature variation. Since the exact temperature dependence is not exactly known the reduction of the anisotropy parameter and micromagnetic exchange takes place through the approximate relations $K(T) \sim [m_e(T)]^3$, $A_{exch}(T) \sim [m_e(T)]^2$ [35, 36]. The spontaneous equilibrium magnetization $m_e(T)$ is taken from the atomistic FePt model presented in [37]. The dependence of saturation magnetization on temperature was modeled using the findings of Okamoto et al. [38]. The MCA was oriented perpendicular to the nanoparticle's square base and the MCA constant was varied. The $Ku = 250$ kJ/m³ in our previous micromagnetic numerical endeavors [28, 29] at 0 K was capable of creating interesting skyrmionic textures in triangular and Reuleaux based FePt nanoelements.

The Finite Differences (FD) micromagnetic simulations were conducted on Nvidia GTX 1080 GPU. The magnetization curves for every production run were investigated by applying external magnetic fields B_{ext} with fixed orientation running parallel to z -direction (the normal to the nanoparticle's square base). The range values

of B_{ext} were +1 T (maximum) and -1 T (minimum) having an external magnetic field step of $\delta B_{ext} = 0.01$ T for the actual magnetic reversal process.

3 Results

3.1 Skyrmion formation and stabilization for the reference nanoparticle

Skyrmion formation and stabilization as a function of the external field, the geometric characteristics of the nanoparticle and of the temperature can be quantitatively characterized by the calculation of the topological invariant S , widely known as skyrmion or winding number [39, 8, 40]. The skyrmion number S is computed using the relation $S = \frac{1}{4\pi} \int_A \mathbf{m} \cdot (\frac{\partial \mathbf{m}}{\partial x} \times \frac{\partial \mathbf{m}}{\partial y}) dA$. The quantity \mathbf{m} is the unit vector of the local magnetization defined as $\mathbf{m} = \mathbf{M}/M_s$ with \mathbf{M} being the magnetization and M_s the saturation magnetization. Magnetization \mathbf{M} is provided by the FD numerical solution of the LLG equation. The skyrmion number S is a physical and topological quantity that measures how many times \mathbf{m} wraps the unit sphere [8, 41, 42]. Surface A is the surface domain of integration and corresponds to the square base of the FePt nanoparticles under investigation.

The skyrmion number S has been computed during the magnetization reversal process as a function of B_{ext} and is shown in **Fig. 1a** for the reference nanoparticle at $T = 300$ K and for $Ku = 130.4$ kJ/m³. As the external field decreases the magnetic system departs from saturation. The magnetization reversal process is closely followed by the external field step of $\delta B_{ext} = 0.01$ T. At first glance for fields down to 0.2 T skyrmion number attains very low values fluctuating around zero. Below 0.2 T the skyrmion number remains fluctuating but attains only positive values indicative for possible starting generation process for a specific micromagnetic configuration. The decrease of the field below 0 T activates a gradual increase of the skyrmion number from $S = 0.1$ to $S = 0.3$ when the external field reaches the $B_{ext} = -0.1$ T value. Infinitesimal decrease of the

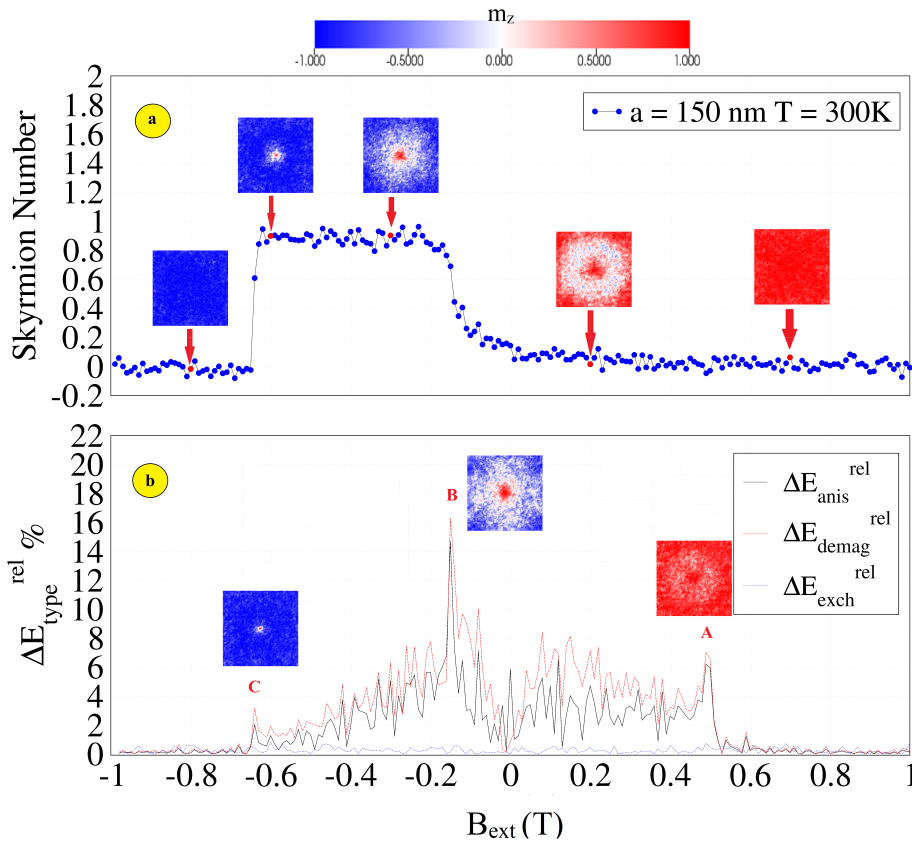


Figure 1: Skyrmion number S as a function of B_{ext} for the reference nanoparticle at 300 K (panel a). The pseudo color which is shown in the depicted micromagnetic configurations refers to the z -component of magnetization (m_z). Relative energy differences as a function of the external field (panel b).

magnetic field below $B_{ext} = -0.1$ T triggers a jump-like discontinuity on skyrmion number. The value of S abruptly increases from $S \approx 0.3$ to $S \approx 1$. Further decrease of the external field does not affect the skyrmion number which develops an extended plateau region with $S \approx 1$ for external field values down to $B_{ext} = -0.63$ T. For magnetic field value below $B_{ext} = -0.63$ T a new abrupt jump-like reduction of skyrmion number S signals

the skyrmion annihilation and the finalization the magnetization reversal process. It is worth mentioning that the existence of thermal field is reflected on the oscillatory behavior of $S(B_{ext})$. These low amplitude oscillations also captured by the micromagnetic configurations visualizations are indicative of the noisy character caused by the thermal field.

The numerical solution of the LLG equation allows the direct representation and inspection of the micromagnetic configurations. These configurations are also shown in **Fig. 1a** for representative values of the external field. It should be noted that the pseudo color used for the micromagnetic configurations refers to z -component of magnetization (m_z). At the initial states of the reversal process the magnetization vectors are aligned parallel to the external field (red colored square in **Fig. 1a**). The micromagnetic configurations for fields $B_{ext} \in [-0.14, 0.2]$ T have a donut-like shape where the core magnetizations point upwards ($+z$) and the magnetizations on the distinct peripheral (rim) domain are tilted having $m_z = 0$ (white color domains in **Figure 1a**) or reversed ($m_z < 0$) (light blue color spots also in **Figure 1a**). The aforementioned magnetization configuration is a magnetic skyrmionium which is a non-topological soliton which has a donut-like out of plane spin texture in magnetic nanoparticles and thin films. It can be viewed as a coalition of two magnetic skyrmions with opposite skyrmion numbers giving a zero total ($S_{skyrmionium} = 0$) [43, 44]. The skyrmionium is considered as a distinct skyrmionic state with particular characteristics [43] heralds the abrupt transition to a clear skyrmionic state ($S = 1$). The formed skyrmion which has a perfect circular shape is a Néel-type skyrmion and as mentioned earlier remains stable for a significant external field range. In the one skyrmion plateau region as the field value decreases from $B_{ext} = -0.16$ T to $B_{ext} = -0.63$ T the actual diameter of the skyrmion also decreases as it can be seen from the representative micromagnetic configurations shown in **Fig. 1a**. The magnetization reversal process is complete when all magnetization vectors are aligned parallel to z -direction (blue colored square in **Fig. 1a**).

The jump discontinuities of skyrmion number as the external field decreases were evident in **Fig. 1a**, albeit the detailed mechanism behind this behavior is not clear. The complex phenomena related to skyrmion formation as well as with the skyrmion number discontinuities could be associated with the rich energetic environment having contributions from demagnetization E_{demag} , exchange E_{exch} and anisotropy E_{anis} energies. In order to shed light on the skyrmion formation the individual energetic contributions [45] were quantified during the magnetization reversal process by computing the absolute relative energy difference $\Delta E_{type}^{rel,i} = \left| \frac{E_{type}^{i+1} - E_{type}^i}{E_{type}^i} \right| \times 100(\%)$ (where *type* stands for *anis*, *exch*, *demag*) between the consecutive (i and $i + 1$) external magnetic field values B_{ext}^i, B_{ext}^{i+1} with ($i = 0, 199$). The values of the relative differences of anisotropy, demagnetization and exchange energies are also shown in **Fig. 1b** as functions of B_{ext} for $Ku = 130.4$ kJ/m³.

Initially, the relative energy differences have very low fluctuating values as external field decreases down to $B_{ext} = 0.5$ T where a discontinuity can be observed for all relative anisotropy and demagnetization energies and clearly can be associated with the creation process of the aforementioned skyrmionium texture. The relative difference values are 6%, 6.5% for $\Delta E_{anis}^{rel}, \Delta E_{demag}^{rel}$, respectively. Gradual decrease of the external field is followed by demagnetization and exchange energy fluctuations for field values down to -0.14 T. Further decrease of the field triggers the skyrmion formation followed by abrupt jump discontinuities in $\Delta E_{anis}^{rel}, \Delta E_{demag}^{rel}$ energies at -0.14 T. The formed skyrmion ($S \approx 1$) at -0.14 T remains stable as the field further decreases with $\Delta E_{anis}^{rel}, \Delta E_{demag}^{rel}$ retaining their fluctuating character showing a clear tendency to attain lower values. At the field value of -0.63 T a new jump discontinuity but with significantly reduced jump amplitude is evident on the relative energy differences shown in **Fig. 1b** which signals the skyrmion annihilation. The relative difference values at the skyrmion annihilation discontinuity are 2%, 3% for anisotropy, demagnetization, respectively. It is worth noting that ΔE_{exch}^{rel} ($< 0.7\%$) remains practically constant with weak fluctuations during the magnetization reversal process while the demagnetization and anisotropy energies play the crucial role to skyrmion formation.

3.2 Skyrmion dependence on nanoparticles's width

For nanoparticles having $a = 150$ nm individual micromagnetic simulations have been conducted at different width (w) values in order to investigate the effect of the nanoparticle's width on the actual skyrmion formation during the magnetization reversal process at the temperature of 300 K. The skyrmion number S as a function of B_{ext} is shown for width values $w = 6 - 36$ nm in **Fig. 2**. Skyrmion can be produced in substantial ranges even for widths down to 12 nm. The present FD micromagnetic simulations reveal that the 12 nm width for nanoparticles having $a = 150$ nm is critical for the creation of skyrmions. Nanoparticles with width values below 12 nm cannot generate complete skyrmions. The $S(B_{ext})$ line shapes for the nanoparticle with $w = 6$ nm substantially deviate from the respective line shapes for higher widths. A smooth increase (still fluctuating) of the skyrmion number as a function of the reducing external magnetic field during the skyrmion's creation process is evident. The nanoparticles with $w = 12 - 36$ nm expose a discontinuous jump-like character for external fields around 0 T. The higher the width the higher the jump-like discontinuity. For all widths the skyrmion annihilation which occurs at different field values is an abrupt process. The skyrmion number reduces

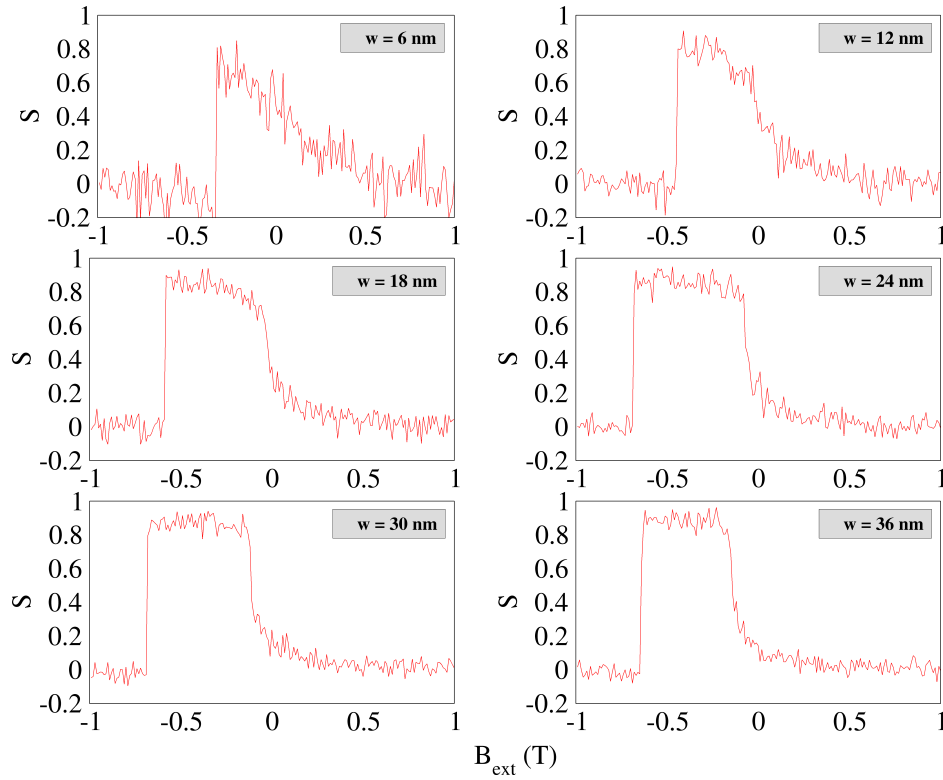


Figure 2: Skyrmion number S as a function of B_{ext} for side value $a = 150$ nm at 300K for geometries having different widths $w = 6, 12, 18, 24, 30, 36$ nm.

from $S \approx 1$ to $S \approx 0$ with no intermediate transition magnetic states.

3.3 Skyrmion dependence on MCA

For the reference nanoparticle ($a = 150$ nm, $w = 36$ nm) simulations have been conducted with varying MCA values $Ku = 78.2 - 234.7$ kJ/m³ while its orientation is set parallel to external field and z -direction. It is interesting the fact that MCA mainly affects the magnetic field range of stabilization of the skyrmion formed and not the skyrmionic state of $S = +1$. Two external fields during the creation ($B_{creationSK}$) and the annihilation ($B_{annihSK}$) of skyrmion were recorded and presented in **Fig. 3**. The $B_{creationSK}$ values of the magnetic field follow a rather weak decrease from -0.12 T to -0.25 T with the gradual increase of the MCA from $Ku = 78.2$ kJ/m³ to $Ku = 234.7$ kJ/m³. The skyrmion annihilation field value of $B_{annihSK}$ exposes a weak but gradual increase from -0.7 T to -0.6 T as the MCA value increases.

The external magnetic field skyrmion's stabilization range $|B_{annihSK} - B_{creationSK}|$ is also monitored in **Fig. 3** exposing a monotonic decrease as MCA value increases from $Ku = 104.3$ and 234.7 kJ/m³. The switching field which is related to initiation of the reversal process is affected by the MCA value showing a clear reduction from 0.5 to 0.3 T with the increase of Ku .

3.4 Skyrmionic states

The topological invariant S reported along with the actual magnetic configurations can provide valuable qualitative information toward the detection and characterization of skyrmionic states. It is very interesting the fact that a variety of micromagnetic skyrmionic states emerges for the square-based FePt nanoparticles. The most commonly detected micromagnetic states are presented along with the respective skyrmion number S in **Fig. 4** and can be assigned to the following categories:

- a, f. Uniform states:** States where the magnetization is uniform and the actual magnetization vectors point all upwards (red color) or all downwards (blue color) [46, 13].
- b, c. Skyrmionium:** A magnetic skyrmionium is a non-topological soliton of a doughnut shape [43, 44].
- d. Domain wall:** A domain wall is a gradual reorientation of individual magnetic moments across a finite distance undergoing an angular displacement of 90° or 180° [47].
- e. Skyrmion with $S = 1$:** State where one skyrmion is formed [40, 28].

From the results presented and the conclusions drawn so far it is clear that skyrmionic textures can be created

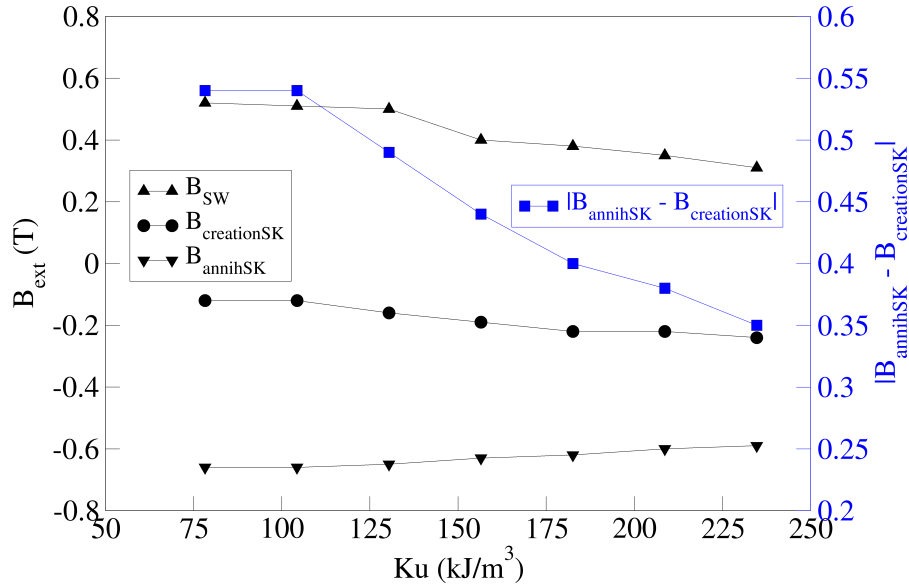


Figure 3: External fields relative to the formation ($B_{creationSK}$) and annihilation ($B_{annihSK}$) as a function of MCA value ($Ku = 78.2 - 234.7$ kJ/m³) for the reference nanoparticle at 300 K.

and stabilized by adjusting the width of the nanoparticle, the MCA value and the temperature of the magnetic system. In addition, the skyrmion number S has been computed during the magnetization reversal for FePt nanoparticles with variable side length. The **Fig. 5** depicts for the temperature of 300 K, $Ku = 130.4$ kJ/m³ and $w = 36$ nm a skyrmionic state diagram constructed by the different values of external field B_{ext} and of the square side length a .

Nanoparticles with side length $a \leq 50$ nm are not capable of hosting stable skyrmionic entities irrespective of the applied external field as can be seen in **Fig. 5**. The restricted surface area affects also the precursor skyrmionium state which is absent in the aforementioned nanoparticles. The precursor skyrmionium states for positive external field values start to appear assisting the development of Néel skyrmions for square bases with $a \geq 60$ nm. The skyrmionium states are present and their development is intimately related to the side length a . The higher the side length the higher the value of the characteristic positive external field value in which they appear. It is very interesting the fact that for the square based parallelepiped geometry the magnetic skyrmions are created for $B_{ext} < 0$ values and in particular for -0.1 T. The detected skyrmions are Néel skyrmions having skyrmion number values in the $[0.79, 0.96]$ interval.

Magnetic nanoparticles that promote not only the creation but also the stabilization of skyrmions in a considerable range of external fields are the nanoparticles with square side length $a \geq 90$ nm. For instance the skyrmions created on the nanoparticles with $a = 90, 100$ nm can be persistent for the field $[-0.4, -0.1]$ T range while the $a = 100, 120, 130$ nm and $a = 140 - 180$ nm the annihilation field is in the vicinity of -0.5 and -0.6 T, respectively. At this point it should be noted that the micromagnetic states represented in **Fig. 5** reveal a

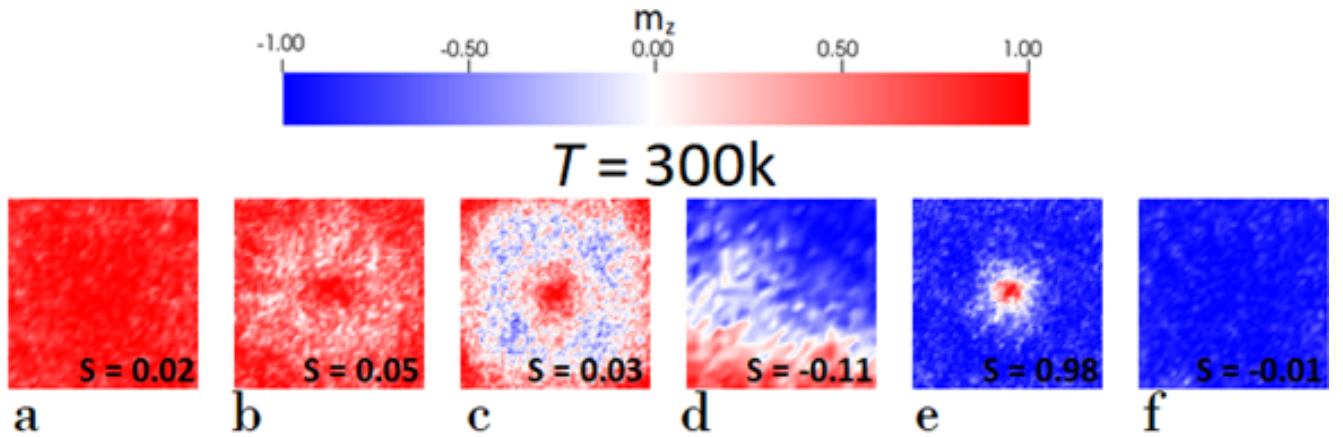


Figure 4: Different states detected for the square base FePt nanoparticle (reference geometry). The states are: (a, f) uniform, (b, c) skyrmionium, (d) domain wall, (e) skyrmion with $S = +1$. MCA value was $Ku = 130.4$ kJ/m³

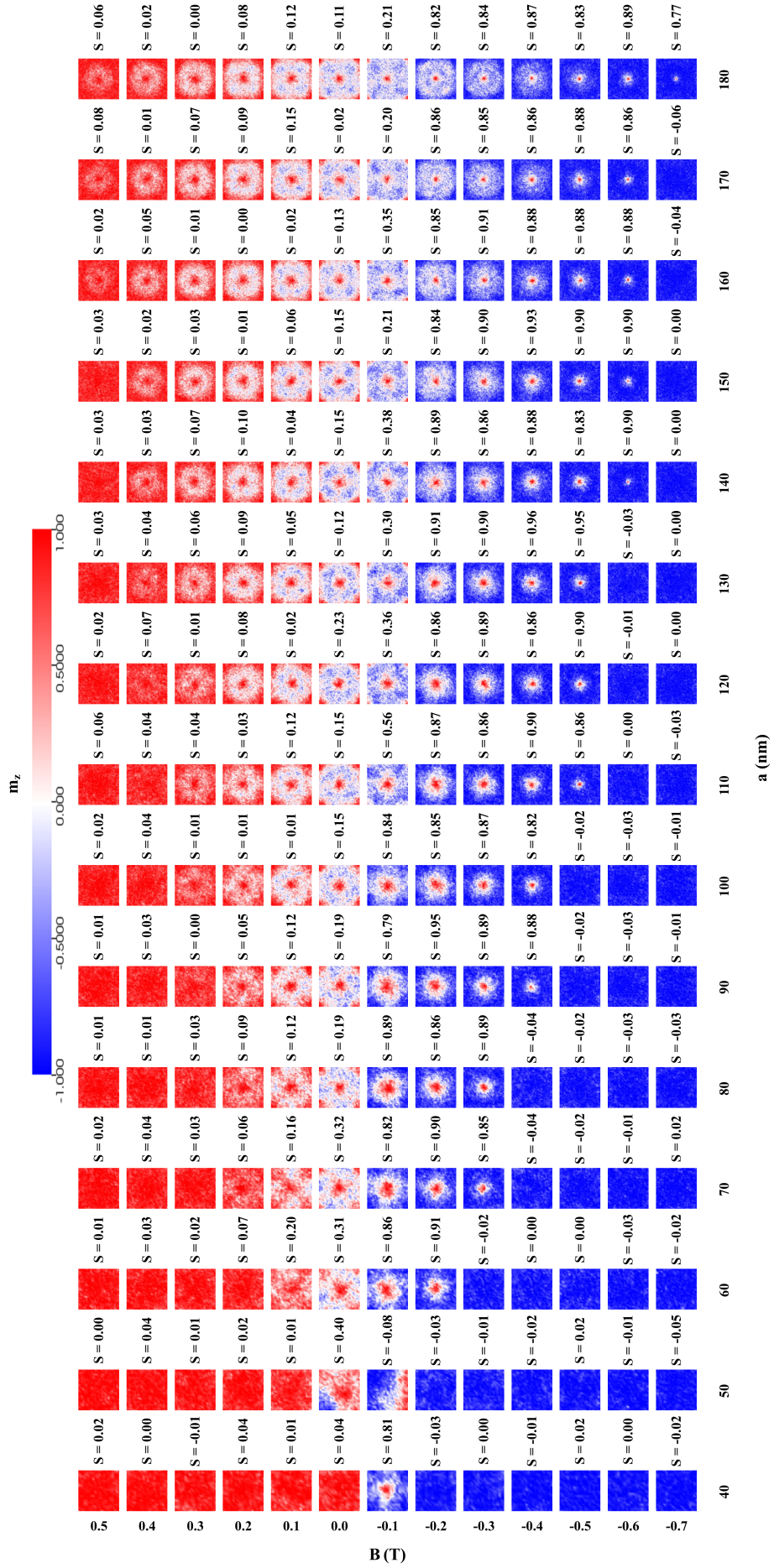


Figure 5: Micromagnetic states revealed at 300 K for the FePt nanoparticle. The color bar refers to the z -component of magnetization (m_z).

significant symmetry with respect to -0.1 T magnetic field. In the majority of the cases the skyrmionic textures of well developed skyrmioniums at positive fields have their mirror -0.1 T axis skyrmion analogue created at negative fields.

3.5 Nanoparticle's internal magnetic structure

Finite Difference micromagnetic simulations can provide rich and detailed information about the magnetization behavior on the surface and in the bulk of nanoparticle. The detected skyrmions on the surface are inevitably related to the magnetization formations on the internal domain of the nanoparticle. The existence of magnetic structure in the internal domain of the magnetic nanoparticle can be revealed by monitoring the magnetization vectors \mathbf{M} for grid points located at different z -levels (xy -cross section) and for yz , xz - cross sections. These cross sections were chosen for micromagnetic systems hosting one Néel skyrmion in order to describe the qualitative characteristics of the actual skyrmionic texture. Néel skyrmion is shown in **Fig. 6** for the reference geometry and for $B_{ext} = -0.3$ T and MCA value $Ku = 130.4$ kJ/m³.

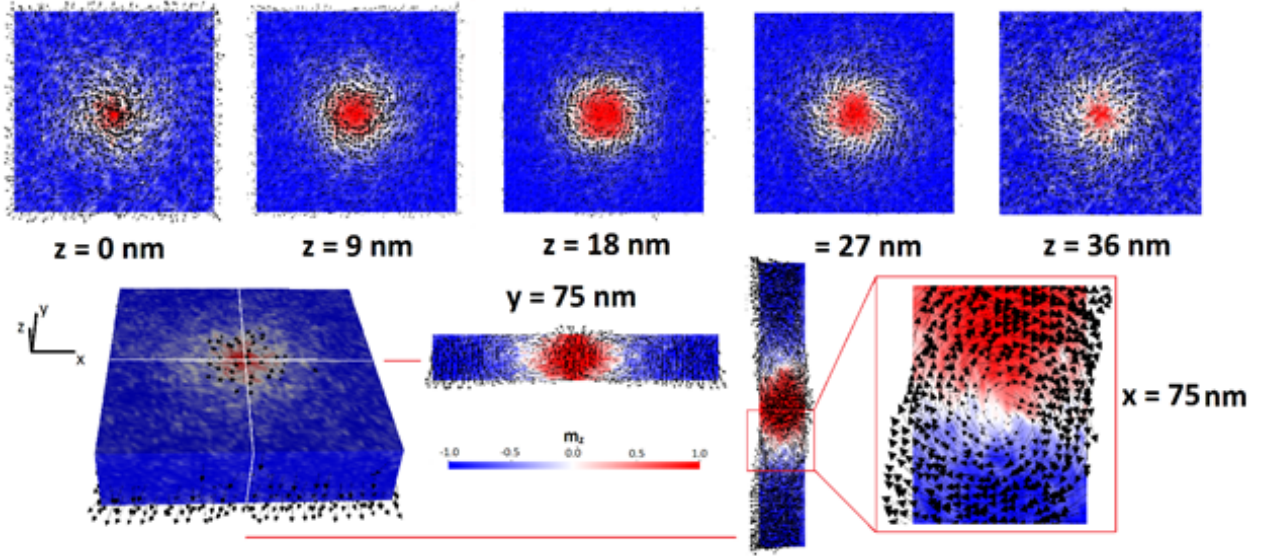


Figure 6: Micromagnetic configurations of a Néel skyrmion at different z -levels ($z = 0, 9, 18, 27, 36$ nm) for $B_{ext} = -0.3$ T and for the reference nanoparticle at 300K. In addition, xz and yz -cross sections sliced at $y = 75, x = 75$ nm respectively are depicted for the square-base parallelepiped geometry of the magnetic nanoparticle. In particular, a magnified domain of the yz -cross section is also shown. The color bar represents the z -component of the magnetization (m_z).

At first glance the presence of magnetic structure is evident for the Néel skyrmion (**Fig. 6**) in all cross sections visualized. In particular, xy -cross sections at $z = 0, 9, 18, 27, 36$ nm reveal skyrmionic configurations appearing in each square z -level and are presented in **Fig. 6**. Interesting is the fact that micromagnetic configurations in the non-surface z -values expose different magnetic characteristics with respect to skyrmions observed on the square bases of the FePt nanoparticle. On the top or bottom surface Néel skyrmions are formed while in the proximity of central bulk region magnetization vectors deviate ($z = 9, 27$ nm of **Fig. 6**) from the Néel skyrmion pattern adopting a more Bloch-type skyrmionic magnetic texture at $z = 18$ nm with vortex type circulating magnetizations. The size of the skyrmionic regions at different z -levels is different with the skyrmion diameter being increased from the surface to the bulk domain of the nanoparticle. The higher diameter can be observed for $z = 18$ nm.

Magnetization configurations represented by the magnetization vector on the nodal points at $z = 0$ nm and $z = 36$ nm are different as can be observed in **Fig. 6**. It should be pointed out that although the two aforementioned z -levels where the magnetization configurations hosting skyrmions look different they are topologically equivalent. This can be justified by the fact that the calculated integrals of the topological density on the two square base areas give the same S .

The present simulation results support the depth dependence of helicity which is an interesting result that has been recently observed experimentally by tomography in systems with bulk skyrmions reported by Zhang et al. [30]. It should be pointed out that although the physics behind skyrmion formation in this system may differ the depth dependence is obviously related to surface effects in both systems. In the present case where skyrmions are created in thin nanoparticles the depth dependence of the demagnetizing field (which has increased z -component near the surfaces [48]) can force the vortex to acquire a Néel character at the surfaces

while maintaining its typical chiral nature at the bulk. The skyrmionic structures observed here depend on the demagnetizing effects which are proportional to the thickness w (as the easy axis remains in-plane) and vanish for low thickness values (<6 nm) as it was shown from the presentation of the current simulation results and discussion. Inevitably, the rich skyrmionic textures and physical phenomena related to the depth dependence of helicity are being suppressed as the thickness becomes comparable to the exchange length (l_{ex}).

At xz -cross section (sliced at $y=75$ nm) which hosts the Néel skyrmion the magnetization vectors develop three distinct regions along the x -direction as exposed in **Fig. 6** with two clear vortex-like magnetization circulations on the interfaces between the regions. In the regions (blue-shaded) located at the right and left corners of xz -cross section magnetizations are pointing downwards with the dimensionless magnetization z -component attaining values $m_z=-1$. Moving away from the corners toward the skyrmionic bulk regions the tilting of magnetizations starts producing the aforementioned vortex formations at the interfaces. At the central bulk region the magnetizations start to align parallel to z -direction pointing upwards ($m_z=+1$).

The yz -cross section is also shown for the Néel in **Fig. 6**. A region hosting magnetization circulations is located at the center of the yz -cross section. Distinct regions hosting parallel magnetizations pointing downwards (blue-shaded region with $m_z=-1$) and upwards (red-shaded region with $m_z=+1$) are evident. Their position follows an alternating fashion blue-red-blue with the interface regions (white region having $m_z=0$) hosting the center of vortex formations.

3.6 Skyrmion's size-diameter

The isolated Néel skyrmions that have been generated on the FePt nanoparticle of square parallelepiped geometries during the reversal process have circular geometry with varying diameter d_{sk} . Their size can be controlled by the magnitude of external field as reported in the recent literature [49] and shown by Finite Element micromagnetics simulations for FePt nanoparticles having reuleaux geometries at 0 K [29]. The skyrmion's size dependence on the external field and on the square base side length a is computed and quantified.

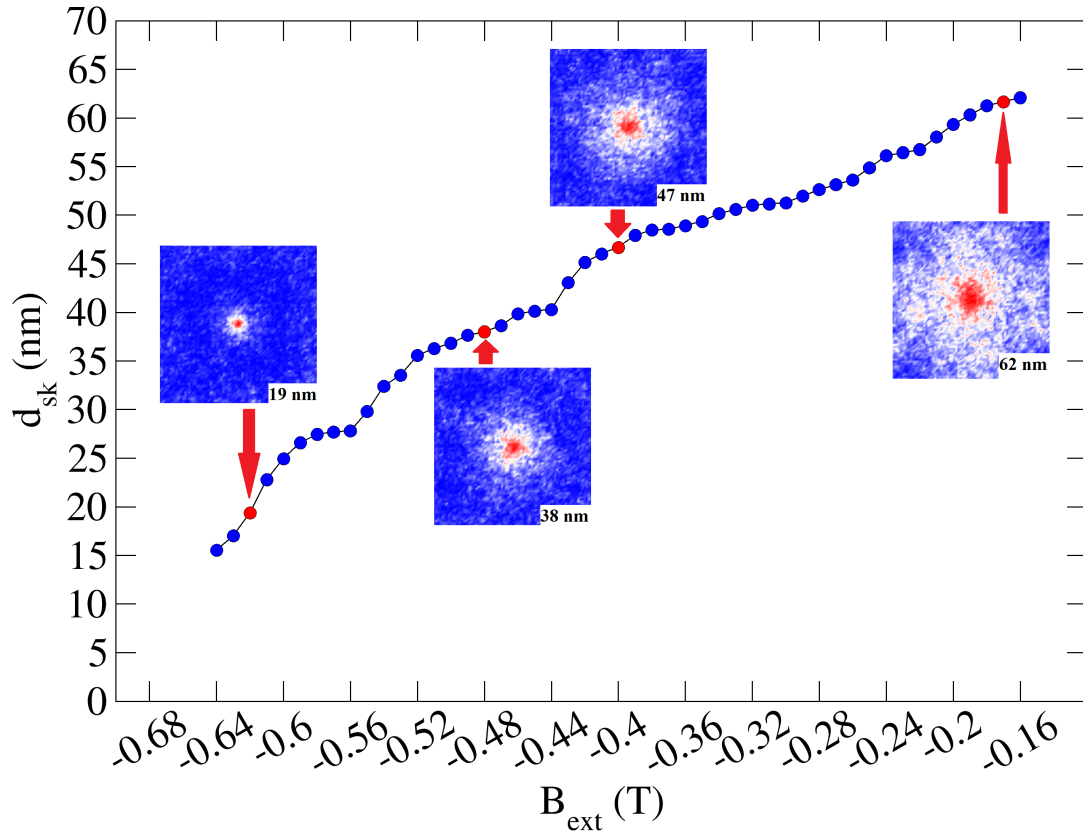


Figure 7: Skyrmion's diameters d_{sk} at $T=300$ K as a function of the applied external field B_{ext} along with representative micromagnetic configurations for the reference nanoparticle ($a = 150$ nm, $w = 36$ nm).

In **Fig. 7** the calculated skyrmion diameter d_{sk} is shown as a function of the external field in the $[-0.64, -0.16]$ T range where $S \approx 1$. The d_{sk} depends more or less linearly on B_{ext} and a linear regression of the simulation points give $d_{sk}(B_{ext}) = 87.074B_{ext} + 78.18$ with a correlation coefficient $R = 0.9817879$. The formed skyrmion at $B_{ext} = -0.16$ T has its maximum diameter value close to 62 nm. Further decrease of the magnetic field causes the gradual decrease of the skyrmion diameter. Just before its annihilation at $B_{ext} = -0.64$ T skyrmion

attains its minimum diameter which is 15 nm. It is evident that the external magnetic field plays a dominant role on the actual size of the Néel-skyrmion.

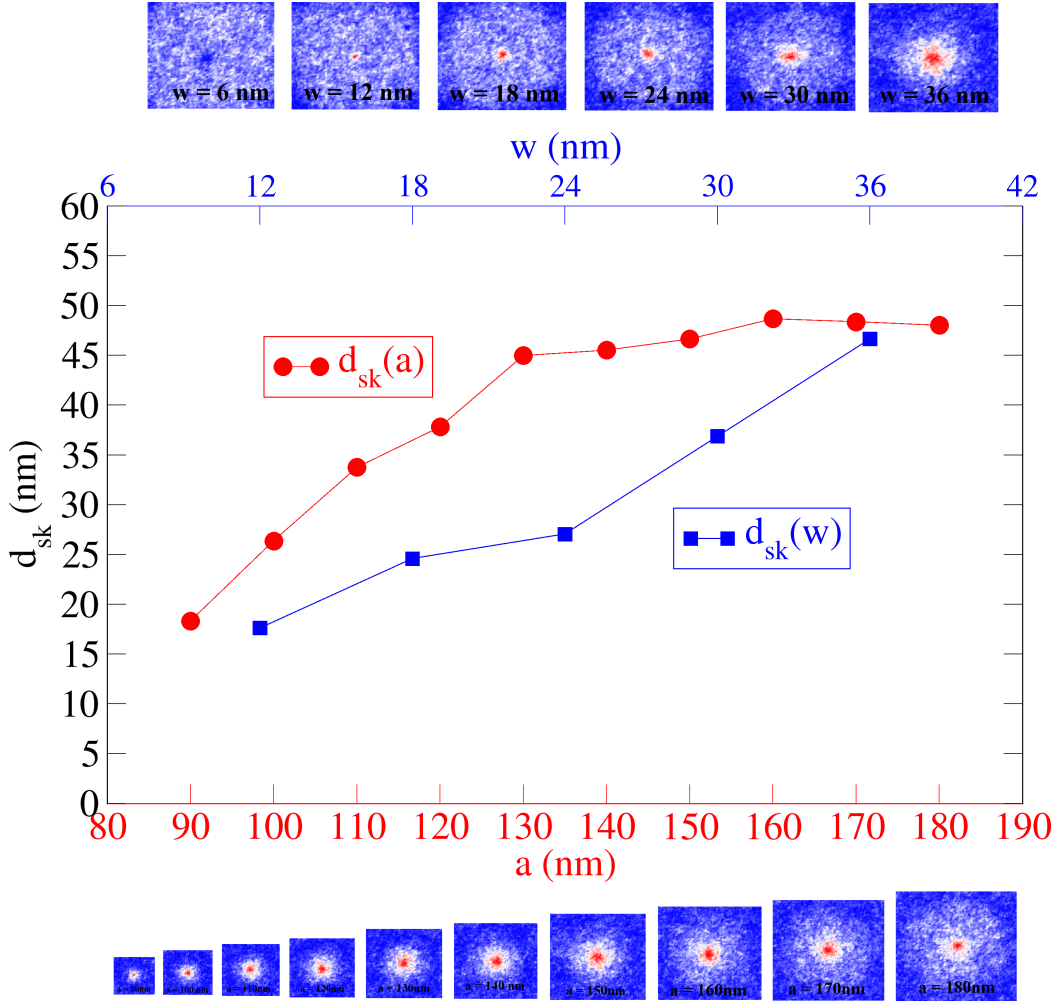


Figure 8: Skyrmion diameters d_{sk} at $T = 300$ K, $Ku = 130.4$ kJ/m³, $B_{ext} = -0.4$ T as a function of nanoparticle's width w in blue color (side length was set to $a = 150$ nm) and as a function of the side length (a) in red color (width length was set to $w = 36$ nm).

The effects of the geometrical characteristics of the nanoparticle on the formed skyrmion size are also studied. Néel skyrmion diameters d_{sk} for $Ku = 130.4$ kJ/m³, external field value $B_{ext} = -0.4$ T at $T = 300$ K were calculated as functions of nanoparticle's width (w) and square's side length (a). In **Fig. 8** $d_{sk}(w)$ functional form is shown in blue color with the side length set to $a = 150$ nm and $d_{sk}(a)$ is presented in red color having constant width $w = 36$ nm. The increase of w is followed by a monotonic increase of d_{sk} values from 17 to 46 nm. This monotonic increase consists of two different linear regions. The first one for nanoparticles with width between 12 and 24 nm ($d_{sk}(w) = 0.78583w + 8.9417$ and $R = 0.9639279$). A second linear region ($d_{sk}(w) = 1.6342w - 12.162$ and $R = 0.9999989$) with higher slope is evident for nanoparticles having 24 to 36 nm width. The width value $w = 24$ nm represents a critical value for the creation of skyrmions with intermediate sizes having diameters close to 27 nm. Regarding the effect of the square side length a of the nanoparticle on the skyrmion diameter also reveals two regimes as can be seen in **Fig. 8**. The first one is linear and follows the increase of d_{sk} from 15 nm to 45 nm as the side length a increases from 90 nm to 150 nm. The second one is a plateau regime in which the skyrmion diameter remains almost constant at 45 nm for square side lengths up to 180 nm.

The skyrmion diameter-size has been calculated at different MCA values for the reference nanoparticle and the results are given in **Fig. 9** for the specific value of $B_{ext} = -0.4$ T. At first glance two regimes exist describing the skyrmion's size dependence on the MCA value. Lower MCA values have a stronger effect on d_{sk} . In particular, as MCA value increases linearly ($d_{sk} = 0.4148Ku - 8.8949$) from 78.2, to 104.3 and finally to 130.4 kJ/m³ the diameter of skyrmion increases attaining the values $d_{sk} \approx 25$, 31, 47 nm, respectively. Further increase of the MCA to values up to $Ku = 234.7$ kJ/m³ does not affect the diameter of the skyrmion and a plateau region is evident with the created skyrmion having $d_{sk} \approx 47.5$ nm.

Finally, the skyrmion diameter for the reference nanoparticle and for $Ku = 130.4$ kJ/m³, $B_{ext} = -0.4$ T has

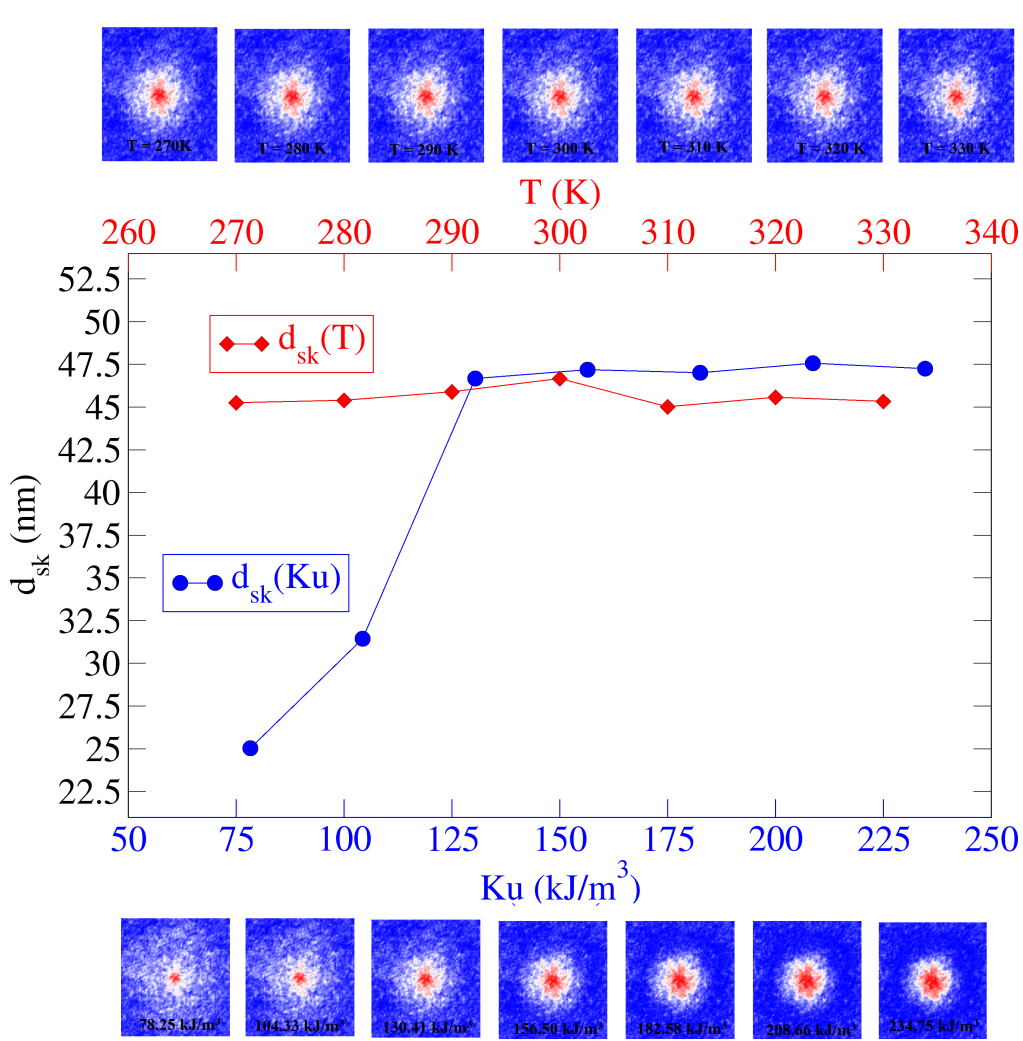


Figure 9: Skyrmion diameters d_{sk} for magnetic field value $B_{ext} = -0.4$ T as a function of temperature T (red horizontal axis) and of MCA Ku (blue horizontal axis) at $T = 300$ K. The reference square-based nanoparticle was used.

been calculated for different temperatures ($d_{sk}(T)$) around 300 K as can be seen also in **Fig. 9**. It is clear that the temperature does not affect the size of the created skyrmion even for temperatures 30 K above or below the room-temperature.

Conclusions

The skyrmion formation in FePt nanoparticles were studied using FD micromagnetic simulations. The adopted micromagnetic model takes into account thermal effects in the form of a Brownian term in the effective field involved in LLG equation and the magnetic material properties were reduced to the temperature range of 270 - 330 K. MCA and external field were set normal to nanoparticle's surface in all conducted numerical simulations. Magnetic skyrmions have been detected during the magnetization reversal process for FePt square-based parallelepiped nanoparticles having different side lengths and widths with MCA value kept constant at $Ku = 130.4\text{ kJ/m}^3$ and $T = 300$ K. Computation of the topological invariant of skyrmion number S accompanied by the visualization of the actual micromagnetic configurations have provided detailed quantitative and qualitative information relative to skyrmion formation and stabilization. Interesting magnetic structures were revealed for particular external magnetic field value ranges. Néel type skyrmionic textures were detected on the outer surfaces coexisting with Bloch-type textures in the bulk of the FePt square-based parallelepiped nanoelements.

The computed sizes of the created Néel skyrmions showed a linear dependence with respect to the external field. At different temperatures and for the external magnetic field value of $B_{ext} = -0.4$ T skyrmions can be generated with a diameter around 45 nm for the reference nanoparticle having $a = 150$ nm. Variation of MCA have a significant effect on the skyrmion diameter only for $Ku \in [78.2, 130.4]\text{ kJ/m}^3$ while for the higher MCA

does not affect the diameter which attains values close to 47.5 nm. The nanoparticles' side length (a) and width (w) affect the skyrmion diameter. The increase of w is followed by an increase of the skyrmion diameter values from 17 to 46 nm. The side length increase can give birth to skyrmions with diameters close to 50 nm. In conjunction with previous finite element studies at 0 K it is clear that magnetic skyrmions can be produced around 300 K in a wide range of external fields and for nanoparticles with different geometrical characteristic dimensions even in the absence of chiral interactions such as Dzyaloshinskii-Moriya for FePt nanoparticles.

Acknowledgments

C. Tyrpenou is supported through the project "Dioni: Computing Infrastructure for Big-Data Processing and Analysis." (MIS No. 5047222) which is implemented under the Action "Reinforcement of the Research and Innovation Infrastructure", funded by the Operational Programme "Competitiveness, Entrepreneurship and Innovation" (NSRF 2014-2020) and co-financed by Greece and the European Union (European Regional Development Fund). V. D. Stavrou was supported through the Operational Programme "Human Resources Development, Education and Lifelong Learning" in the context of the project "Strengthening Human Resources Research Potential via Doctorate Research" (MIS-5000432), implemented by the State Scholarships Foundation (IKY) co-financed by Greece and the European Union (European Social Fund-ESF). We would like to thank Mr. K. Dimakopoulos for technical support.

References

- [1] N. S. Kiselev, A. N. Bogdanov, and R. Schafer and U. K. Robler. Chiral skyrmions in thin magnetic films: new objects for magnetic storage technologies. *Journal of Applied Physics D*, 44:392001, 2011.
- [2] N. Romming, C. Hanneken, M. Menzel, J. E. Bickel, B. Wolter, K. von Bergmann, A. Kubetzka, and R. Wiesendanger. Writing and deleting single magnetic skyrmions. *Science*, 341:636–639, 2013.
- [3] G. Yu, P. Upadhyaya, Q. Shao, H. Wu, G. Yin, X. Li, C. He, W. Jiang, X. Han, P. K. Amiri, and Kang L. W. Room-temperature skyrmion shift device for memory application. *Nano letters*, 17(1):261–268, 2016.
- [4] K. Everschor-Sitte, J. Masell, R. M. Reeve, and M. Kläui. Perspective: Magnetic skyrmions-overview of recent progress in an active research field. *Journal of Applied Physics*, 124(24):240901, 2018.
- [5] X. Zhang, Y. Zhou, K. M. Song, T. E. Park, J. Xia, M. Ezawa, X. Liu, W. Zhao, G. Zhao, and S. Woo. Skyrmion-electronics: writing, deleting, reading and processing magnetic skyrmions toward spintronic applications. *Journal of Physics: Condensed Matter*, 32(14):143001, jan 2020.
- [6] A. Fert, N. Reyren, and V. Cros. Magnetic skyrmions: advances in physics and potential applications. *Nature Reviews Materials*, 2(7):17031, 2017.
- [7] J. Seidel. *Topological structures in ferroic materials: domain walls, vortices and skyrmions*. Springer series in materials science. Springer Cham, Cham, Switzerland, 2016.
- [8] J. Ping Liu, Zhidong Zhang, and Guoping Zhao. *Skyrmions: Topological Structures, Properties, and Applications*. CRC PRESS, Boca Raton, 2017.
- [9] F. Büttner, I. Lemesch, and G. S. D. Beach. Theory of isolated magnetic skyrmions: From fundamentals to room temperature applications. *Scientific Reports*, 8:4464, 2018.
- [10] C. Moreau-Luchaire, C. Moutafis, N. Reyren, J. Sampaio, C. A. F. Vaz, N. Van Horne, K. Bouzehouane, K. Garcia, C. Deranlot, P. Warnicke, P. Wohlhüter, J.M. George, M. Weigand, J. Raabe, V. Cros, and A. Fert. Additive interfacial chiral interaction in multilayers for stabilization of small individual skyrmions at room temperature. *Nature Nanotechnology*, 11:444–448, 2016.
- [11] D. Zhao, L. Zhang, I. A. Malik, M. Liao, W. Cui, X. Cai, C. Zheng, L. Li, X. Hu, D. Zhang, J. Zhang, X. Chen, W. Jiang, and Q. Xue. Observation of unconventional anomalous hall effect in epitaxial CrTe thin films. *Nano Research*, 11(6):3116–3121, Jun 2018.
- [12] M. V. Sapozhnikov, O. V. Ermolaeva, E. V. Skorokhodov, N. S. Gusev, and M. N. Drozdov. Magnetic skyrmions in thickness-modulated films. *JETP Letters*, 107(6):364–368, Mar 2018.
- [13] Pepper R. A., Beg M., Cortés-Ortuño D., Kluyver T., Bisotti M. A., Carey R., Vousden M., Albert M., Wang W., Hovorka O., and Fangohr H. Skyrmion states in thin confined polygonal nanostructures. *Journal of Applied Physics*, 123:093903, 2018.

- [14] A. F. Schäffer, L. Rózsa, J. Berakdar, E. Y. Vedmedenko, and R. Wiesendanger. Stochastic dynamics and pattern formation of geometrically confined skyrmions. *Communications Physics*, 72:1–10, 2019.
- [15] R. Keesman, A. O. Leonov, P. van Dieten, S. Buhbrandt, G. T. Barkema, L. Fritz, and R. A. Duine. Degeneracies and fluctuations of néel skyrmions in confined geometries. *Phys. Rev. B*, 92:134405, Oct 2015.
- [16] J. Sampaio, V. Cros, S. Rohart, A. Thiaville, and A. Fert. Nucleation, stability and current-induced motion of isolated magnetic skyrmions in nanostructures. *Nature Nanotechnology*, 8:839–844, 2013.
- [17] Beg M., Carey R., Wang W., Cortés-Ortuño D., Vousden M., Bisotti M. A., Albert M., Chernyshenko D., Hovorka O., Stamps R. L., and Fangohr H. Ground state search, hysteretic behaviour, and reversal mechanism of skyrmionic textures in confined helimagnetic nanostructures. *Scientific Reports*, 5(17137):1–14, November 2015.
- [18] A. O. Leonov, Y. Togawa, T. L. Monchesky, A. N. Bogdanov, J. Kishine, Y. Kousaka, M. Miyagawa, T. Koyama, J. Akimitsu, Ts. Koyama, K. Harada, S. Mori, D. McGrouther, R. Lamb, M. Krajnak, S. McVitie, R. L. Stamps, and K. Inoue. Chiral surface twists and skyrmion stability in nanolayers of cubic helimagnets. *Phys. Rev. Lett.*, 117:087202, Aug 2016.
- [19] D. Maccariello, W. Legrand, N. Reyren, K. Garcia, K. Bouzehouane, S. Collin, V. Cros, and A. Fert. Electrical detection of single magnetic skyrmions in metallic multilayers at room temperature. *Nature Nanotechnology*, 13:233–237, 2018.
- [20] W. Legrand, D. Maccariello, F. Ajejas, S. Collin, A. Vecchiola, K. Bouzehouane, N. Reyren, V. Cros, and A. Fert. Room-temperature stabilization of antiferromagnetic skyrmions in synthetic antiferromagnets. *Nature Materials*, 19:1–9, 2020.
- [21] S. D. Pollard, J. A. Garlow, J. Yu, Z. Wang, Y. Zhu, and H. Yang. Observation of stable Néel skyrmions in Co/Pd multilayers with lorentz transmission electron microscopy. *Nature Communications*, 8:14761, 2017.
- [22] O. Boulle, J. Vogel, H. Yang, S. Pizzini, D. De Souza Chaves, A. Locatelli, T.O. Montes, A. Sala, L.D. Buda-Prejbeanu, O. Klein, M. Belmeguenai, Y. Roussigne, A. Stashkevich, S. Mourad Cherif, L. Aballe, M. Foerster, M. Chshiev, S. Auffret, I.M. Miron, and G. Gaudin. Room-temperature chiral magnetic skyrmions in ultrathin magnetic nanostructures. *Nature Nanotechnology*, 11(5):449–454, 2016.
- [23] A. Hrabec, M. Sampaio, J. Belmeguenai, I. Gross, R. Weil, S. M. Cherif, A. Stashkevich, V. Jacques, A. Thiaville, and S. Rohart. Current-induced skyrmion generation and dynamics in symmetric bilayers. *Nature Communications*, 8:15765, 2017.
- [24] J. Brandao, D.A. Dugato, R.L. Seeger, J.C. Denardin, T.J.A. Mori, and J.C. Cezar. Observation of magnetic skyrmions in unpatterned symmetric multilayers at room temperature and zero magnetic field. *Scientific Reports*, 9(1):4144, 2019.
- [25] S. Husain, N. Sisodia, A.K. Chaurasiya, A. Kumar, J.P. Singh, B.S. Yadav, S. Akansel, K.H. Chae, A. Barman, P.K. Muduli, P. Svedlindh, and S. Chaudhary. Observation of skyrmions at room temperature in Co₂FeAl heusler alloy ultrathin film heterostructures. *Scientific Reports*, 9(1):1085, 2019.
- [26] C.T. Ma, Y. Xie, H. Sheng, A.W. Ghosh, and S.J. Poon. Robust formation of ultrasmall room-temperature Néel skyrmions in amorphous ferrimagnets from atomistic simulations. *Scientific Reports*, 9(1):9964, 2019.
- [27] V. D. Stavrou, L. N. Gergidis, A. Markou, A. Charalambopoulos, and I. Panagiotopoulos. Micromagnetics of triangular thin film nanoelements. *Journal of Magnetism and Magnetic Materials*, 401:716–723, 2016.
- [28] L. N. Gergidis, V. D. Stavrou, D. Kourounis, and I. Panagiotopoulos. Micromagnetic simulations study of skyrmions in magnetic FePt nanoelements. *Journal of Magnetism and Magnetic Materials*, 481:111 – 121, 2019.
- [29] V. D. Stavrou, D. Kourounis, K. Dimakopoulos, I. Panagiotopoulos, and L. N. Gergidis. Magnetic skyrmions in FePt nanoparticles having reuleaux 3D geometry: a micromagnetic simulation study. *Nanoscale*, 11(42):20102–20114, 2019.
- [30] S. Zhang, G. van der Laan, J. Müller, L. Heinen, M. Garst, A. Bauer, H. Berger, C. Pfleiderer, and T. Hesjedal. Reciprocal space tomography of 3d skyrmion lattice order in a chiral magnet. *Proceedings of the National Academy of Sciences*, 115(25):6386–6391, 2018.
- [31] W. F. Brown. Thermal fluctuations of a single-domain particle. *Phys. Rev.*, 130:1677–1686, Jun 1963.

- [32] A. Vansteenkiste, J. Leliaert, M. Dvornik, M. Helsen, F. Garcia-Sanchez, and B. Van Waeyenberge. The design and verification of mumax3. *AIP Advances*, 4(10):107133, 2014.
- [33] J. Leliaert, M. Dvornik, J. Mulkers, J. De Clercq, M. Milosevic, and B. Van Waeyenberge. Fast micromagnetic simulations on GPU : recent advances made with mumax3. *Journal of Physics D-Applied Physics*, 51(12):31, 2018.
- [34] A. Markou, K. G. Beltsios, L. N. Gergidis, I. Panagiotopoulos, T. Bakas, K. Ellinas, A. Tserepi, L. Stoleriu, R. Tanasa, and A. Stancu. Magnetization reversal in triangular L10-FePt nanoislands. *Journal of Magnetism and Magnetic Materials*, 344:224–229, 2013.
- [35] U. Atxitia, O. Chubykalo-Fesenko, N. Kazantseva, D. Hinzke, U. Nowak, and R. W. Chantrell. Micromagnetic modeling of laser-induced magnetization dynamics using the landau-lifshitz-bloch equation. *Applied Physics Letters*, 91(23):232507, 2007.
- [36] H.B. Callen and E. Callen. The present status of the temperature dependence of magnetocrystalline anisotropy, and the $l(l+1)2$ power law. *Journal of Physics and Chemistry of Solids*, 27(8):1271–1285, 1966.
- [37] N. Kazantseva, D. Hinzke, U. Nowak, R. W. Chantrell, U. Atxitia, and O. Chubykalo-Fesenko. Towards multiscale modeling of magnetic materials: Simulations of fept. *Phys. Rev. B*, 77:184428, 2008.
- [38] S. Okamoto, N. Kikuchi, O. Kitakami, T. Miyazaki, Y. Shimada, and K. Fukamichi. Chemical-order-dependent magnetic anisotropy and exchange stiffness constant of FePt (001) epitaxial films. *Phys. Rev. B*, 66:024413, 2002.
- [39] T. H. R. Skyrme. A unified field theory of mesons and baryons. *Nuclear Physics*, 31:556–569, April 1962.
- [40] K. Palotás. High-resolution combined tunneling electron charge and spin transport theory of Néel and Bloch skyrmions. *Phys. Rev. B*, 98:094409, Sep 2018.
- [41] J.W. Yoo, S.J. Lee, J.H. Moon, and K.J. Lee. Phase diagram of a single skyrmion in magnetic nanowires. *IEEE Transactions on Magnetics*, 50:1500504, 2014.
- [42] T. Fischbacher, M. Franchin, G. Bordignon, and H. Fangohr. Ground state search, hysteretic behaviour, and reversal mechanism of skyrmionic textures in confined helimagnetic nanostructures. *Scientific Reports*, 5:6784, 2015.
- [43] X. Zhang, J. Xia, Y. Zhou, D. Wang, X. Liu, W. Zhao, and M. Ezawa. Control and manipulation of a magnetic skyrmionium in nanostructures. *Phys. Rev. B*, 94:094420, Sep 2016.
- [44] S. Zhang, F. Kronast, G. van der Laan, and T. Hesjedal. Real-space observation of skyrmionium in a ferromagnet-magnetic topological insulator heterostructure. *Nano Letters*, 18(2):1057–1063, 2018.
- [45] Y. Y. Dai, H. Wang, P. Tao, T. Yang, W. J. Ren, and Z. D. Zhang. Skyrmion ground state and gyration of skyrmions in magnetic nanodisks without the Dzyaloshinsky-Moriya interaction. *Phys. Rev. B*, 88:054403, Aug 2013.
- [46] C. P. Chui, F. Ma, and Y. Zhou. Geometrical and physical conditions for skyrmion stability in a nanowire. *AIP Advances*, 5(4):047141, 2015.
- [47] J. M. D. Coey. *Magnetism and Magnetic Materials*. Cambridge University Press, 2010.
- [48] K. Tang, H.W. Zhang, Q.Y. Wen, and Z.Y. Zhong. Demagnetization field of ferromagnetic equilateral triangular prisms. *Physica B: Condensed Matter*, 363(1):96 – 101, 2005.
- [49] X. S. Wang, H. Y. Yuan, and X. R. Wang. A theory on skyrmion size. *Communications Physics*, 1:31, 2018.